**Atmospheric
Chemistry
and Physics**

NO$_2$ climatology in the northern subtropical region: diurnal, seasonal and interannual variability

M. Gil[1], M. Yela[1], L. N. Gunn[2], A. Richter[3], I. Alonso[1], M. P. Chipperfield[2], E. Cuevas[4], J. Iglesias[1], M. Navarro[1], O. Puentedura[1], and S. Rodríguez[1]

[1]Area de Investigación e Instrumentación Atmosférica, INTA, Torrejón de Ardoz, Spain
[2]Institute for Atmospheric Science, School of Earth and Environment, University of Leeds, Leeds, UK
[3]Institute of Environmental Physics, University of Bremen, Bremen, Germany
[4]Centro de Investigación Atmosférica de Izaña, INM, Sta. Cruz de Tenerife, Spain

Abstract. Daily NO$_2$ vertical column density (VCD) has been routinely measured by zenith sky spectroscopy at the subtropical station of Izaña (28° N, 16° W) since 1993 in the framework of the Network for the Detection of Atmospheric Composition Change (NDACC). Based on 14 years of data the first low latitude NO$_2$ VCD climatology has been established and the main characteristics from short timescales of one day to interannual variability are presented. Instrumental descriptions and different sources of errors are described in detail. The observed diurnal cycle follows that expected by gas-phase NO$_x$ chemistry, as can be shown by the good agreement with a vertically integrated chemical box model, and is modulated by solar radiation. The seasonal evolution departs from the phase of the hours of daylight, indicating the signature of upper stratospheric temperature changes. From the data record (1993–2006) no significant long-term trends in NO$_2$ VCD can be inferred. Comparison of the ground-based data sets with nadir-viewing satellite spectrometers shows excellent agreement for SCIAMACHY with differences between both datasets of 1.1%. GOME displays unrealistic features with the largest discrepancies during summer. The ground-based data are compared with long-term output of the SLIMCAT 3-D chemical transport model (CTM). The basic model, forced by ECMWF (ERA-40) analyses, captures the observed NO$_2$ annual cycle but significantly underestimates the spring/summer maximum (by 12% at sunset and up to 25% at sunrise). In a model run which uses assimilation of satellite CH$_4$ profiles to constrain the model long-lived tracers the agreement is significantly improved. This improvement in modelled column NO$_2$ is due to better modelled NO$_y$ profiles and points to transport errors in the ECMWF ERA-40 reanalyses.

1 Introduction

NO$_2$ plays an important role in the chemistry of ozone from the mid stratosphere to the mesosphere through catalytic reactions:

$$NO + O_3 \rightarrow NO_2 + O_2 \qquad (1)$$

$$NO_2 + O \rightarrow NO + O_2 \qquad (2)$$

$$\text{Net: } O_3 + O \rightarrow 2O_2 \qquad (3)$$

The NO$_x$ contribution to the overall O$_3$ equilibrium depends on latitude, altitude and season. The primary source of stratospheric active nitrogen is N$_2$O (e.g. see Minschwaner et al., 1993). In the middle and upper stratosphere N$_2$O is converted to NO by reaction with excited oxygen atoms O(^{1}D) produced mainly by UV photolysis of O$_3$. Measurements have shown a steady increase in atmospheric N$_2$O over the last two decades of 2.2–2.6% per decade (WMO, 2007). While the chemistry of the NO$_y$ family has been well established over recent decades, long-term NO$_2$ observations display positive trends exceeding that of N$_2$O. Liley et al. (2000) analysed the longest available visible spectroscopy dataset (Lauder, New Zealand) and found an increase of 5±1% for the period 1980–1999, some 2% larger than the estimated trend in N$_2$O. The same rate of increase (+5.2±3.2% per decade) was obtained by Rinsland et al. (2003) for Kitt Peak (32° N) using FTIR spectrometer data. Struthers et al. (2004) extended the Liley et al. (2000) work by comparing Lauder

and Arrival Heights (Antarctica, 78° S) data with a three-dimensional coupled chemistry-climate model (CCM). They again found a greater rate of increase of NO$_2$ compared with N$_2$O both in the measurements and the model.

Differential optical absorption spectrometry (DOAS) in the visible range has been used extensively for ground-based measurements of NO$_2$ vertical column density (VCD) since the pioneering work of Brewer (1973) and Noxon (1975), and further improvements by Solomon et al. (1987) and others. Since the late 1980s/1990s zenith spectrometers have been deployed at remote locations around the globe for studies of stratospheric NO$_2$. Most of them are integrated into the Network for Detection of Atmospheric Composition Change (NDACC), formerly NDSC, follow a measurement protocol and participate in regular intercomparisons for quality assurance (http://www.ndsc.ncep.noaa.gov/). These data have helped establish a better understanding of nitrogen oxides stratospheric behaviour in the extra-tropical region. In 1993 Izaña (28° N) initiated its routine measurement programme for NO$_2$, later extended to O$_3$ and BrO. In the early 1990s four stations were also set up in the framework of the Systeme d'Analyse par Observation Zenithale (SAOZ) network in the Southern Hemisphere (http://www.aero.jussieu.fr/themes/CA/Reseau_SAOZ.html). Recently, two more were added to the BREDOM network (http://www.iup.physik.uni-bremen.de/doas/groundbased_data.htm). However, long records in the tropical latitude belt are still scarce and no comprehensive long-term low latitude NO$_2$ measurements have been reported to date.

In the last decade, the technique has been successfully extended to satellites instruments such as GOME (ESA, 1995), SCIAMACHY (Bovensman et al., 1999) and OMI (Dover et al., 2005) and will continue in the years to come with the GOME-2, a set of units on board of the operational METOP series. While polar orbiting satellites offer the advantage of global coverage, no study of stratospheric diurnal variation is possible since they scan low latitude regions once per day at best. Additionally, orbiting instruments require validation from the ground to establish the optimum settings and detect potential degradation with time. Ground-based quality controlled instrumentation provides independent measurements, stable in time, which are extremely useful for validating orbiting instruments. The UV-Vis spectrometer network has contributed to the NO$_2$ validation of satellite instruments such as GOME (e.g. Lambert et al., 1998; Richter et al., 2000) on board the ERS-2, and extensively to SCIAMACHY (e.g. Lambert et al., 2004; Richter et al., 2004; Piters et al., 2006; Lambert et al., 2007) and MIPAS (e.g. Hendrick et al., 2004; Wetzel et al., 2007) on the ENVISAT platform.

Here we report the behaviour of the NO$_2$ column over the high altitude subtropical station of Izaña (28° N, 16° W, Tenerife, Canary Islands, 2370 m a.s.l.) on different time scales, from diurnal to interannual, based on 14 years of data. Ground-based observational data are compared to models and satellite measurements for the same location, constituting a limited low-latitude NO$_2$ climatology for the period 1993–2006.

2 Passive DOAS at zenith

The technique used is based on measurement of atmospheric absorption of solar radiation in selected wavelength bands where NO$_2$ has a structured cross-section. For stratospheric observations the instrument is pointed at the zenith sky. Under these conditions, the equivalent photon path (EPP), or radiation slant path, for a given wavelength is defined as the single path that corresponds to the sum of all paths contributing to the observed zenith radiation weighted by the intensity of each one. At twilight, the scattering point of the EPP occurs in the stratosphere. The slant path from the top of the atmosphere to the scattering point is enhanced as the sun moves to larger solar zenith angles (sza), while below the scattering point radiation comes from the vertical. As a consequence, the stratospheric contribution of the NO$_2$ absorption is amplified compared to the tropospheric one (Solomon et al., 1987).

The logarithm of this equivalent twilight spectrum, ideally ratioed to an extraterrestrial spectrum, yields the optical depth of the absorbers, providing that the Lambert-Beer equation applies which is the case in an optically thin atmosphere. In practice, the extraterrestrial spectrum is substituted by a spectrum measured at high sun (so called reference spectrum). The measured NO$_2$ column is, in fact, the difference in NO$_2$ between twilight and high sun EPP and it is called the Differential Slant Column Density (DSCD). The high sun spectrum contains an unknown amount of NO$_2$ which has to be estimated and added afterwards to obtain the NO$_2$ Slant Column Density (SCD).

The DOAS at zenith technique requires that all absorbers are known in advance and that their absorption cross-sections are known in the spectral range selected. DSCDs are derived by least squares fitting (i.e. Vandaele et al., 2005) using:

$$\left(\frac{d}{dN_i}\right)\left|\ln\left[\frac{I(a\lambda+b)}{I_{\text{ref}}(\lambda)}\right]+\sum\{\sigma_i(\lambda)*\text{DSCD}_i\}+P(\lambda)\right|^2$$

$$=\varepsilon \text{ (minimum)} \tag{4}$$

Where $I(\lambda)$ is the twilight spectrum. Parameters a and b account for spectral squeeze and shift due to small changes in the spectrograph and are obtained by iterative approximations until the minimum residual is reached. $I_{\text{ref}}(\lambda)$ is the reference spectrum at high sun after alignment using the Fraunhofer lines present in the solar spectrum. σ_i are the differential absorption cross-sections and $P(\lambda)$ is a polynomial function accounting for scattering. To convert the spectral observations to vertical column density (VCD) a further two-step process is required. First, the amount of the NO$_2$ density contained in the reference spectrum must be computed and

added to the DSCD, and then the vertical column conversion is performed by dividing by the Air Mass Factor (AMF) coefficients.

2.1 Reference content and AMF calculations

The amount of gas contained in the reference spectrum in dynamically controlled species can be obtained as the intercept of a linear fit by the classical Langley plot method:

$$\text{Ref} = \text{VCD} * \text{AMF (sza)} - \text{SCD (sza)} \tag{5}$$

where VCD is the vertical column density of the gas under consideration and SCD (sza) is the amount retrieved from the observations. AMF (sza) is mainly a function of solar zenith angle (sza) but also dependent, to some extent, on the shape of the vertical profile of the gas under consideration. Ref is the amount contained in the zenith reference spectrum at high sun. It can be retrieved as the intercept of the linear fit under the assumption of no concentration changes during the period of the measurements. Other species of short photochemical lifetime, e.g. NO$_2$, undergo significant changes throughout the day, and the constant column assumption is not valid. Consequently the representation of AMF versus slant column departs from a straight line.

For these short-lived species the so-called modified AMF must be used instead (Lee et al., 1994). These AMFs are obtained by including a coefficient C (sza)=VCD$_0$/VCD (sza), where VCD (sza) comes from a photochemical box model for the appropriate season. VCD$_0$ is the vertical column at the sza where the reference spectrum is recorded. The correction assumes that the actual NO$_2$ diurnal variation is proportional to the NO$_2$ predicted by the model. The reference content can then be estimated by:

$$\text{Ref} = \text{VCD} * \text{AMF (sza)} * \text{C (sza)} - \text{SCD (sza)} \tag{6}$$

The reference spectrum can be used for many years if the spectrograph does not change its specifications, and the Langley plot is computed only once per reference.

3 The station

The Global Atmospheric Watch (GAW) Izaña station, managed by the Instituto Nacional de Meteorología (INM, Spain), is located at 28°18′ N, 16°29′ W on Tenerife (Canary Islands), 300 km from the African west coast at an altitude of 2370 m a.s.l. The Canary Islands are below the descending branch of the Hadley Cell which favours a large-scale high stability catabatic flow regime, resulting in a large number of clear-sky days. The appearance of deep lows and cut-off lows, which could favour stratosphere-troposphere exchange, is limited to winter time. The station is above a quasi-permanent trade wind inversion well established between 800 and 1500 m a.s.l., only absent during some episodes in winter. As a consequence, the station

is under free-troposphere conditions most of the time, precluding pollution from the Sta. Cruz and Puerto de la Cruz coastal towns from reaching the station, except on occasions associated with the passing of low pressure systems. In-situ annual mean NO$_2$ during twilight are of 115 and 473 pptv for a.m. and p.m. respectively (Y. Gonzalez, personal communication). The summer-autumn stratospheric circulation is essentially zonal. Air-masses originate at 20–25° N with little latitudinal variation (Schneider et al., 2005). During winter there is a large variation in the origin of the air masses arriving at the station due to planetary wave activity. Occasionally polar stratospheric air-masses reach the station (Yela, 1999).

3.1 Instrumentation

Two instruments contribute to the data record. In May 1993 a scanning spectrometer (EVA) was installed on the terrace of the observatory for twilight measurements between 88°–92° in the 430–450 nm spectral range. It is based on a Jobin-Yvon H20 monochromator with a ruled grating of 1200 grooves/mm and a photomultiplier tube Hammamatsu R212-UH blue enhanced as the detector. Spectral resolution is 1 nm FWHM and the sampling path is 0.1 nm. A full spectrum is taken in 1.7 s and 30 spectra per measurement are accumulated to improve the signal-to-noise ratio. The instrument is located outdoors in a thermostatised housing. Light reaches the spectrograph by a 45° angle mirror. The instrument takes one measurement per 0.5° of sza between 88° and 92°.

In December 1998 an advanced visible spectrograph (RASAS) was installed. The instrument is based on an EGG&1453A 1024 photodiode array (PDA) detector controlled by an EGG 1461 on a Jarrel-Ash Monospec 18 spectrograph. Scattered light at zenith is collected by a baffled cylinder through a quartz fibre bundle with the inner end rectangle-shaped acting as 100 μm entrance slit. A flat-ruled diffraction grating of 600 grooves/mm provides a spectral range of 340–600 nm for NO$_2$ and O$_3$ observations with an average FWHM resolution of 1.3 nm. The spectrograph and detector are housed in a thermostatised hermetic container keeping the spectrograph at a constant temperature of 15±0.2°C, thus maintaining the alignment of the spectra with time. The detector is operated at −35°C by means of a 2-step peltier and external assistance of a circulating chiller at −10° C. A continuous supply of dry nitrogen from a generator prevents ice formation on the detector window. In-house control software keeps the assembly in operation. Measurements are carried out in continuous mode from 94° sza at dawn to 94° at sunset skipping the central hours of the day whenever the sza is smaller than 45° to avoid spectra perturbations due to reflections in the entrance baffle and direct sun. Typical daytime integration time in clear sky is 2.5 s, increasing to 25 s at 90° sza. The instrument is programmed to integrate spectra during the time required for the sun to move 0.2°, therefore about 500 spectra are collected

Table 1. Summary of main specifications of spectrometers used in this work.

Spectrometers technical specifications			
	EVA	RASAS	ARTIST
Type of spectrometer	Scanning	Spectrograph	Spectrograph
Monochromator	Jobin-Yvon H20	Jarrel Ash Monospec 18	Jobin Yvon TRIAX 180
Difraction grating	Ruled, 1200 grooves/mm	Ruled, 600 grooves/mm	Holographic, 900 grooves/nm
Slit width	250 μm	100 μm	100 μm
Detector type	Photomultiplier	Photodiode array (PDA)	Photodiode array (PDA)
Detector model	HAMAMATSU R212-UH	EGG&1453A 1024-PDA at -35°C	Princeton Instruments PDA 1024 at -40°C
Controller	Home made	EGG 1461	Princeton Instruments STS 121
FWHM	1.25 nm	1.3 nm	0.6 nm
Spectral range	430–450 nm	340–600 nm	325–460 nm
Fitting window for NO$_2$	430–450 nm	425–540 nm	425–450 nm
Detector full depth STN	4000	4100	>10 000
Oversampling factor	Sampling path 0.1 nm	5 pixel/nm	7.7 pixel/nm
Light collection	45° angle mirror	Quartz fibre bundle	Quartz fibre bundle
FOV (half angle)	8.5°	6.5°	3.2°
Measurement period	Since 1993	Since 1998	Since 2001
Location	Outdoor	Indoor	Indoor
Thermostatic control	Yes	Yes (15±0.2°C)	Yes (14±0.2°C)
External chiller	No	Yes ($T=-10$°C)	Yes ($T=0$°C)
Measurement SZA range	88° to 92° every half degree	a.m. 94°to 45° p.m. 45° to 94°	a.m. 94° to 45° p.m. 45° to 94°
SZA range for mean twilight	89° to 91°	89° to 91°	89° to 91°
Typical integration time	1.7 s /spectrum	2.5–25 s at SZA 90°	3–50 s at SZA 90°
Accumulation	30 spectra/measurement	During time required by the sun to move 0.2° SZA at SZA 90°	During time required by sun to move 0.2° SZA at SZA 90°
Typical shift	$\pm2e-2$ nm	$\pm5e-3$ nm	$\pm2.5e-3$ nm
Typical stretch	$\pm4e-3$ nm/range	$\pm7.5e-2$ nm/range	$\pm1.5e-3$ nm/range

everyday. Midnight spectra are recorded everyday for dark current checking. Spectral resolution is measured periodically by monitoring a low-pressure Hg lamp and whenever an increase in the errors is observed.

Short-term studies and diurnal evolution are carried out with a third instrument. The ARTIST spectrometer is optimized for BrO measurements covering the 325–460 nm range at 0.6 nm resolution FWHM. The detector is a Princeton PDA1024 operating at -40°C controlled by a ST121 unit. Light collection is essentially identical to RASAS except for a narrower Field Of View (FOV). Lower detector noise and high instrumental stability result in a signal-to-noise 2 times better than the RASAS instrument. The entrance FOV's (half angle) are 8.5°, 6.5°, and 3.2° for EVA, RASAS, and ARTIST, respectively. Instrumental details are summarised in Table 1.

The UV-Vis spectrometer RASAS has been operating on a routine basis since late 1998 and ARTIST since 2001. Both are NDACC (formerly NDSC) -qualified instruments. INTA has participated in the OHP 1996 (Roscoe et al., 1999) and Andoya 2003 (Vandaele et al., 2005) NDACC intercomparison exercises.

3.2 Data and settings

Fourteen years of data have been used in the analysis. Due to a refurbishment of the Izaña observatory from 1998 to 2003 the spectrometers were installed in a container separated from the main building. From time to time they suffered failures due to power supply interruptions and high dust produced by the surrounding working machines that reached the spectrograph through the nitrogen generator. In October 2003 the spectrometers were moved again to the upper floor of the main building tower significantly improving the laboratory temperature control and power, resulting in almost no gaps in the data since that date.

NO$_2$ from the scanning EVA spectrometer is retrieved in the 433–448.5 nm range. The operational RASAS analysis makes use of a larger spectral interval (435–540 nm) for simultaneous retrieval of NO$_2$ and O$_3$ columns. NO$_2$ from the ARTIST is evaluated in the 425–450 nm range. The NO$_2$ absorption cross-sections in the visible are highly structured, Gaussian in shape, with a large number of optically active transitions with irregular fine structure superimposed, due to the strong coupling between the ground and first excited

electronic states (Orphal, 2002). Doppler broadening, due to thermal motion of the molecules, and pressure broadening are irrelevant for the retrieval at the spectral resolution used in our instruments.

In order to homogenise the results, cross sections used are those defined as standard in the Andoya NDACC (NDSC) intercomparison (Vandaele et al., 2005). A set of 6 cross-sections have been included in the analysis; O$_3$ at 223 K (Bogumil et al., 2001), NO$_2$ at 220 K (Vandaele et al., 1998), H$_2$O from Hitran database (2000) and O$_4$ at room temperature by Greenblatt et al. (1990). The Raman scattering cross-section was generated by the Windoas package (Fayt and Van Roozendael, 2001) from the Raman theory. Finally, the inverse of the reference spectrum was included as a pseudo-cross-section to account for stray light inside the spectrograph and detector residual dark current. Figure 1 shows an example of clear-sky fitting results at twilight for all three instruments. The ARTIST performance yields very low residuals (2.5–3.5×10^{14} mole/cm^2) while RASAS and EVA perform at a similar level (6–7×10^{14} molec/cm^2).

Air Mass Factors were computed by the INTA single scattering radiative transfer model (Sarkissian et al., 1995a) at 440 and 500 nm, for EVA and RASAS, respectively, using the procedure described in Sarkissian et al. (1995b). An ozonesonde climatology from Tenerife was used for O$_3$ and temperature profiles. A single set of AMFs has been used for all seasons since both NO$_2$ and stratospheric temperature annual variations in subtropical regions are small. No aerosols have been included in the calculations.

Stratospheric annual mean temperatures over Izaña for the same 1993–2005 period have been obtained from the monthly mean assimilation data provided by the British Atmospheric Data Centre calculated using the daily analyses from the United Kingdom Met Office. The original data set includes temperature on the standard UARS pressure levels, from surface to 0.316 hPa, on a 2.5° latitude by 3.75° longitude global grid. The data assimilation system used data from operational meteorological observations.

3.3 Errors

Uncertainties in UV-Vis spectrometry at zenith during twilight come from four sources: errors in the retrieval, uncertainty in NO$_2$ cross-sections, uncertainty in the reference content and AMF calculations. Typical fitting errors range from 1–2 % under clear skies and 2–3% in cloudy conditions. The uncertainty in the Vandaele et al. (1998) NO$_2$ cross-sections is estimated to be 2% or better. These cross-sections are recommended as standard by Orphal (2002) in his comprehensive review. Uncertainty in the amount of the reference content from modified-Langley plots, estimated as the standard deviation of the intercept for a cluster of days, accounts for another 2%. The AMF depends on the shape of the NO$_2$ profile distribution. The NO$_2$ profile changes from sunrise to sunset and from winter to summer due to photo-
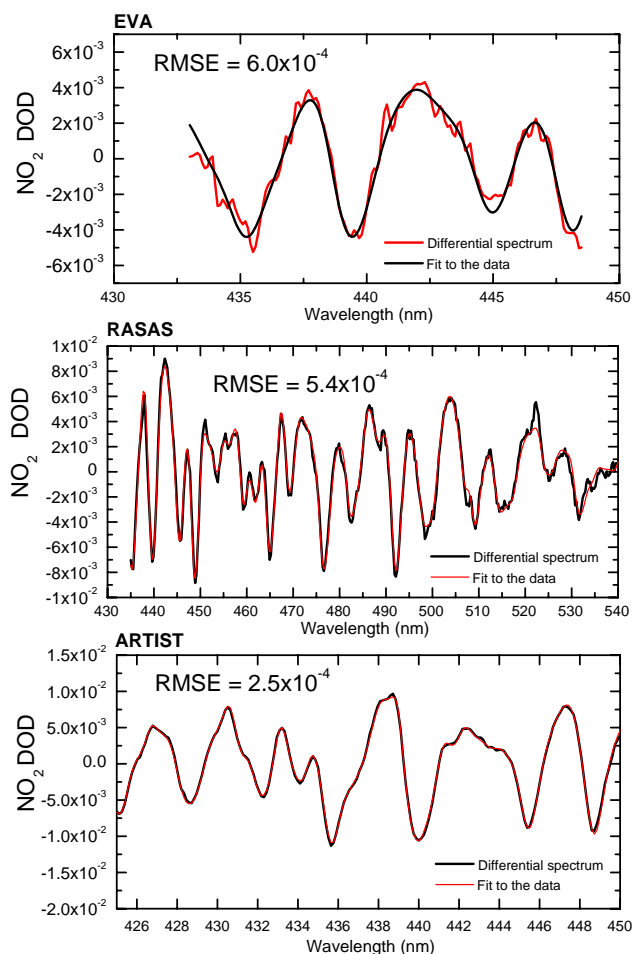

Fig. 1. Examples of spectral fits for the EVA, RASAS and ARTIST ground-based spectrometers for the standard NO$_2$ retrieval ranges. No smoothing has been applied to the spectra.

chemistry. Accurate VCD AMFs require day-to-day calculations based on realistic NO$_2$ profiles. For practical reasons a single AMF-set has been used all the year round. The AMF has been computed for the AFGL profiles for the tropical scenario by the INTA fully spherical single-scattering radiative transfer code. The model was run for sunrise and sunset during the solstices to estimate the error introduced by this approximation. In this case profiles have been extracted from the NO$_2$ harmonic climatology by Lambert et al. (2000) based on HALOE v19 and POAM-III data. AMF differences between this climatology and the AFGL-tropical used as reference for summer-winter and am-pm in the 89°–91° sza range, are of the order of 5%. The error due to single scattering approximation AMF at the retrieved sza and wavelengths is below 1%. The overall uncertainty due to the AMF is estimated to be 6–7%.

The differential cross-section of NO$_2$ in the visible range depends on temperature. Retrievals using stratospheric temperatures (i.e. 220 K) yield too low NO$_2$ when the actual
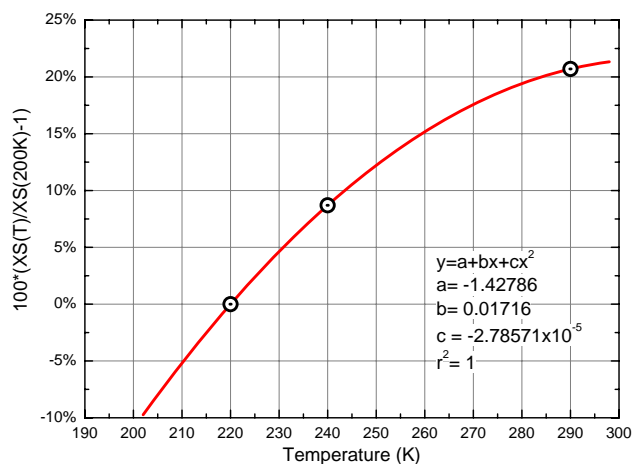
Fig. 2. Magnitude (in percent) of the errors in the RASAS spectral range if temperatures are different from 220 K, based on Vandaele et al. (1998) cross sections.

Fig. 3. Effective temperatures above Izaña for the solstices from a radiosonde climatology and the AFGL tropical model.

temperature is higher. Figure 2 shows the magnitude of the error as a function of the effective temperature of the atmosphere for the 435–540 nm spectral range based on the Vandaele et al. (1998) cross-sections. The NO$_2$ effective temperature at a given sza can be defined as the mean temperature of the atmosphere weighted by the NO$_2$ concentration at each layer contributing to the total observed rays in the same way as the O$_3$ effective temperature (Bernhard et al., 2005):

$$\text{Teff}(\text{sza}) = \frac{\int_0^{\text{top}} \text{NO}_2(z) \cdot \text{WF}(\text{sza}, z) \cdot T(z)dz}{\int_0^{\text{top}} \text{NO}_2(z) \cdot \text{WF}(\text{sza}, z)dz} \quad (7)$$

where WF(sza,z) are the normalized weighting functions for each altitude. Since the altitude of the maximum scattering is strongly dependent on the sza during twilight a large change in the NO$_2$ effective temperature is observed at high sza (Fig. 3). If a unique NO$_2$ cross-section is used during the day an underestimation of 10 to 13% occurs at noon due to this effect. Except for the investigation of the diurnal variation, only spectra at around 90° sza have been used in this work. Under these conditions, the NO$_2$ effective temperature essentially matches the cross-section temperature (220 K). About ±1–2% error can be produced due to changes in the NO$_2$ effective temperature at twilight during the year, which is not corrected in the presented data.

The FOV of the instrument also has an impact on the retrieved columns. The observed spectrum results from the integration of rays of different directions within the FOV, while the column is referred to an ideal pure zenith line. We can define an effective path, $\overline{R}$, dependent on the semi FOV (α) as:

$$\overline{R} = \frac{\sec \alpha - 1}{\ln(\sec \alpha)} \quad (8)$$

For the FOV's used in our instruments $\overline{R}$ is less than 1% larger than the pure vertical or, in other words, we expect an
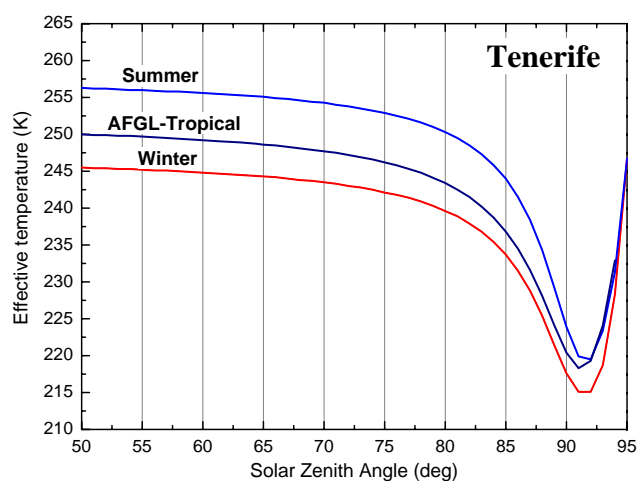
underestimation of the column of less than 1% due to this effect. The overall uncertainty in the data considering all mentioned effects is estimated to be 12–14%

3.4 Homogenization of the dataset

In order to minimise the impact of the switch from scanning instrument (EVA) to PDA-based spectrograph (RASAS) on the data record, both instruments have been kept in parallel operation at Izaña for an extended time period. In Fig. 4a the VCDs from EVA and RASAS are shown for the twilight mean between 89° and 91° for the overlapping years 2000 and 2001. Cross-correlation shows no deviation from unity in the slope (Fig. 4b), the standard deviation being 1.6×10^{14} molec/cm^2. When distinguishing between a.m. and p.m. data the slope changes slightly to 0.96 and 1.03, respectively. As a consequence of the excellent overlap between instruments, a complete 1993–2006 NO$_2$ record was created without the use of any kind of correction factors.

4　SLIMCAT 3-D model

SLIMCAT is an off-line 3-D chemical transport model (CTM) described in detail by Chipperfield (1999) and Chipperfield (2006). The model has been used in many studies of stratospheric chemistry and has been shown to perform well (e.g. Feng et al., 2006). The model contains a gas-phase stratospheric chemistry scheme along with a treatment of heterogeneous chemistry on liquid aerosols and liquid/solid polar stratospheric clouds (PSCs). Horizontal winds and temperatures are specified using meteorological analyses (e.g. from European Centre for Medium-Range Weather Forecasts (ECMWF)) while vertical transport in the stratosphere is diagnosed from calculated heating rates.
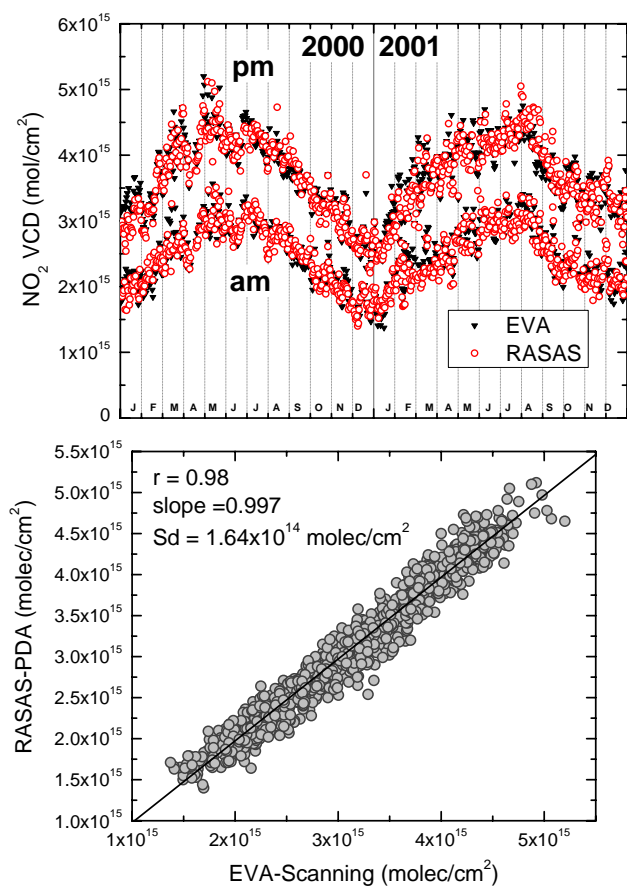
Fig. 4. EVA and RASAS NO$_2$ VCD for the years 2000–2001 **(a)** and cross-correlation **(b)**.

In this study the model was run at a resolution of $7.5° \times 7.5°$ with 24 hybrid $\sigma - \theta$ levels from the surface to approximately 60 km. Two runs were performed; the first (run A) was a simulation with free-running chemistry. The model was integrated from 1977 until 2006 using ECMWF analyses (ERA-40 up to 2001, then operational). Chemical boundary conditions were applied by specifying surface mixing ratios of source gases based on past observations (WMO, 2003). In this run the distribution of chemical species is therefore determined by the modelled chemistry and transport. A second model run (run B) was performed which included chemical data assimilation. Run B started in 1991 (initialised from run A) but with assimilation of HALOE O$_3$, CH$_4$, H$_2$O and HCl. The method of chemical data assimilation used in this model is described in Chipperfield et al. (2002) and uses the sequential technique of Khattatov et al. (2000) along with preservation of model-predicted tracer-tracer correlations. In effect, the assimilation of the long-lived tracer CH$_4$ constrains all of the modelled long-lived tracers and serves to correct errors in the modelled transport (as provided by the forcing analyses).

Model output was saved every 2 days (at 00:00 UT) interpolated to the location of Tenerife. A stacked chemical
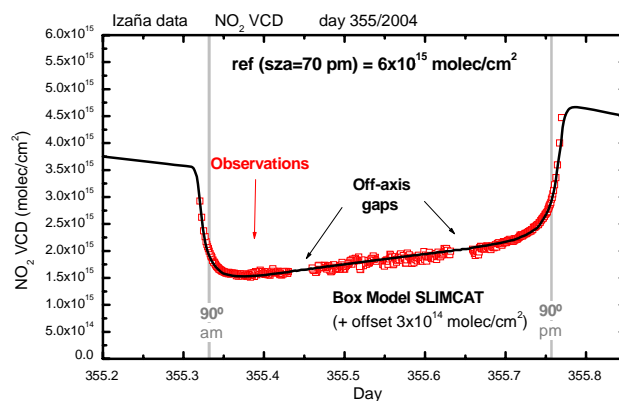

Fig. 5. NO$_2$ VCD during a day (red squares) versus output from the SLIMCAT photochemical box model.

box model was then run to obtain model output at the correct time of day for comparison with the observations (sunrise and sunset at 90° sza).

5 Results

5.1 Diurnal variations

Although optimized for twilight observations, DOAS visible spectroscopy can be used to study the diurnal evolution of the NO$_2$ in unpolluted environments. Measurements at low SZA are challenging since they are highly sensitive to instrumental noise, accuracy in air mass factors and atmospheric conditions. Additionally, the impact of the uncertainty in the reference content to the VCD, which is small at twilight, increases at low SZA since measured SCD approach zero towards noon. A wrong estimation of the absorber content in the reference results in a strong diurnal variation with either too large an increase (excess) or too low (defect of reference content).

For these reasons we have selected days with extremely low aerosol content resulting in very large signal to noise ratio. In Fig. 5 an example is shown for winter solstice. The diurnal variation has been constrained by considering that, once the day conditions are established, NO$_2$ VCD increases linearly during the day, between 80° morning and evening, essentially due to photodissociation of N$_2$O$_5$ (Solomon et al., 1986). A value of 6×10^{15} molec cm^{-2} in the reference content (sza=70° p.m.) is obtained in this way. Measurements start at sza of 93.3° a.m. and end at 93.6° p.m. when the sky illumination is too low. Data gaps between 65° and 70° in a.m. and p.m. are due to the instrument scheduling configuration for off-axis measurements. The diurnal cycle has been simulated for the same day and latitude by vertically integrating in 1-min steps the output profile of a photochemical box model derived from the SLIMCAT 3D CTM (Denis et al., 2005). A fixed offset of 3×10^{14} molec cm^{-2} is added
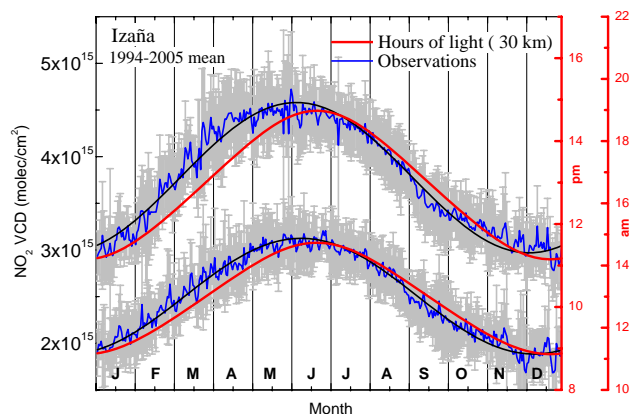
Fig. 6. Climatological seasonal waves for a.m. and p.m. data (blue lines). Gray error bars represent one standard deviation. The red curves show hours of available sunlight at 30 km on two different scales to show departures from pure photochemical equilibrium. Black lines are the result of the fit of primary and secondary waves (see text).

to the model data to fit the observations. Other tested days provide similar results although these kind of observations are restricted to winter period when days of extremely low aerosol optical depths (AOD<0.03 at 500 nm) occur. The good agreement in the diurnal behaviour provides observational evidence of the accuracy of the model NO$_y$ chemistry at low latitudes.

5.2 Seasonal variability

The climatological seasonal wave has been obtained by taking the mean for each day of all the years considered (Fig. 6). Mean annual values are of 2.51×10^{15} and 3.79×10^{15} molec cm^{-2} for a.m. and p.m., respectively. Although strongly modulated by photochemistry through the number of sunlit hours in the stratosphere, a spring-autumn asymmetry occurs. The maximum departure from pure photochemical control takes place at 13–13.5 h of light (March–October) (Fig. 7). The asymmetry can be described by a secondary wave which is phase-shifted by 3 months with respect to the primary one, having an amplitude of 2.8×10^{14} and 4.5×10^{14} molec cm^{-2} for the a.m. and p.m. data, respectively. A relative contribution to the VCD of about 6% during the equinoxes (Fig. 8a) results in a shifting of the NO$_2$ VCD maximum/minimum toward spring/autumn. The secondary wave has been found to be highly correlated to the temperature in the upper stratosphere. The sign of the correlation is opposite to that expected from an artefact resulting from temperature changes not treated in the retrieval. Figure 8b displays the correlation between the NO$_2$ secondary wave contribution to the VCD and the mean temperature from UKMO for the same time period (1993–2006), showing how the observed modulation is dominated by the layer above 5 hPa
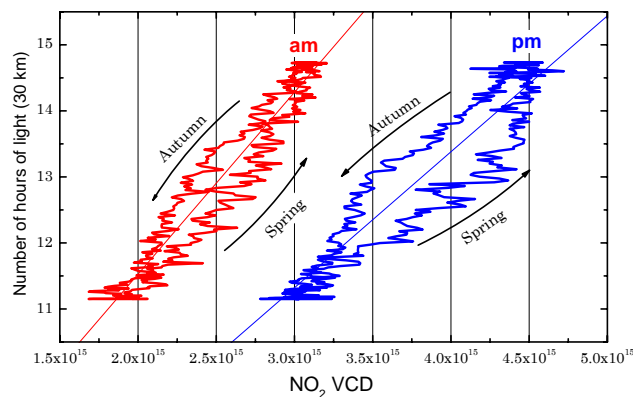

Fig. 7. The NO$_2$ VCD versus hours of available sunlight at 30 km showing a spring-autumn asymmetry.

($\sim$36 km) where the correlation coefficient is over 0.85. The change in NO$_2$ due to temperature can be estimated for daytime by computing the ratio

$$\frac{NO}{NO_2} \approx \frac{J_{NO_2} + k_1[O]}{k_2[O_3]} \tag{9}$$

where k_1 and k_2 are the reaction constants of NO$_2$+O$\rightarrow$NO+O$_2$ and NO+O$_3$$\rightarrow$NO$_2$+O$_2$, respectively. The ratio NO/NO$_2$ decreases as temperature increases resulting in an almost linear NO$_2$ increase of 1.5%/K in the stratosphere for J, [O] and [O$_3$] typical of a tropical atmosphere. This corresponds to 6% for the 4 K amplitude of the temperature wave in the upper stratosphere, in good agreement with observations.

5.3 Interannual variability

The monthly mean column NO$_2$ data record since 1993 is shown in Fig. 9a. The column displays an increase in the first years due to the recovery from stratosphere partial denoxification after the Mt. Pinatubo eruption in 1991, observed as a general feature in ground-based datasets (Johnston et al., 1992; Koike et al., 1993; Van Roozendael et al., 1997; Liley et al., 2000). However, other interannual variability can also be seen from the observational record. From 2002 onwards a decrease in the amplitude of the annual wave is observed. Departures from the seasonal mean (Fig. 9b) can be due to a number of effects such as changes in the meridional component of dominant winds in the mid stratosphere due to drifting in quasi-stationary waves or the QBO, changes in temperature, etc. An interpretation of these features requires a detailed knowledge of the dynamics and chemistry of the region and is out of the scope of this work. Trends are not obvious from the figure and in any case are not statistically significant.
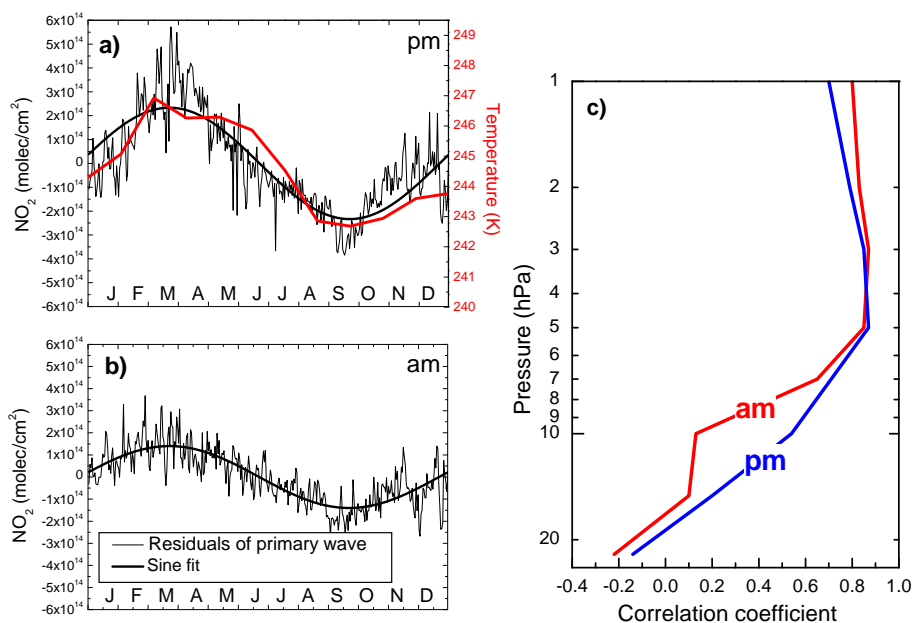
Fig. 8. (a) Amplitude of the secondary wave and temperature at 5 hPa (∼36 km). **(b)** Correlation between secondary waves and upper stratosphere temperature.

5.4 Ground-based versus satellite

Ground-based a.m. NO$_2$ VCDs have been compared to GOME (ERS-2) and SCIAMACHY (ENVISAT) VCD data retrieved at the University of Bremen (Richter et al., 2005a, Richter et al., 2005b) updated to version 2.0. The satellite data are based on DOAS retrievals performed in the 425–450 nm range with essentially the same settings as used for the ground-based instruments, except for the NO$_2$ cross-sections. For GOME, the NO$_2$ cross-sections of (Burrows et al., 1998) at 241 K were used, while for SCIAMACHY the Bogumil et al. (2003) values at 243 K were used. Due to the lack of simultaneity between ground-based and satellite measurements, the diurnal change of the VCD must be taken into account for a proper intercomparison (Lambert et al., 2004; Sussmann et al., 2005). According to box model results and observations (see Fig. 5), the NO$_2$ VCD continues to decrease due to photodissociation well after the 90° a.m. DOAS measurements. The column recovers during daytime at a rate of 6×10^{13} molec/cm^2/h and equals the a.m. twilight after noon (fractional day 0.58 and 0.62 in winter and summer, respectively). ENVISAT overpasses the station at around 10:00 Solar Local Time (SLT) or fractional day 0.42, therefore values 2.3 to 2.9×10^{14} molec/cm^2 lower in SCIAMACHY data would be expected due to this effect. GOME overpass is half an hour later and the difference with the ground-based data should be 3×10^{13} molec/cm^2 less. A fraction of it would be compensated by the smaller NO$_2$ column observed by the ground-based spectrograph as compared to the satellite due to the height of the observatory. Additional

uncertainties result from the different line of sight of both instruments. Maximum sensitivity of ground-based zenith instrumentation at dawn occurs some 200 km in the direction towards sunrise. While this difference must be considered at high latitudes where NO$_2$ zonal gradients can be significant in winter due to asymmetry of the polar vortex (Solomon et al., 1994), its contribution at tropical regions is within the error bars and has not been taken into account in this work.

Figure 10 displays the satellite NO$_2$ VCD superimposed on the ground-based DOAS. One year of overlap between GOME and SCIAMACHY shows consistency in magnitudes between both instruments. When compared to the ground-based data, SCIAMACHY shows excellent agreement while GOME data produces too low summer values and the annual maximum shifted towards spring. SCIAMACHY minus ground-based differences are 1.1% on average (Fig. 11a) with a moderate standard deviation of 2.2×10^{14} molec/cm^2. GOME yields lower values (−9.4%) and larger standard deviation 3.0×10^{14} molec/cm^2 (Fig. 11b).

As discussed above, the satellite data should be slightly lower than the ground-based measurements as result of the photochemical change of NO$_2$ over the day. However, this is not the case for SCIAMACHY while for GOME the underestimate is very strong. For SCIAMACHY, the most probable reason is the use of NO$_2$ cross-sections at 243 K instead of 220 K, which leads to a systematic overestimation of about 6% (2×10^{14} molec/cm^2 in summer, 1.2×10^{14} molec/cm^2 in winter). For GOME NO$_2$ columns, a spectral interference pattern induced by the diffuser plate used for irradiance measurements prevents the use of the solar measurements as
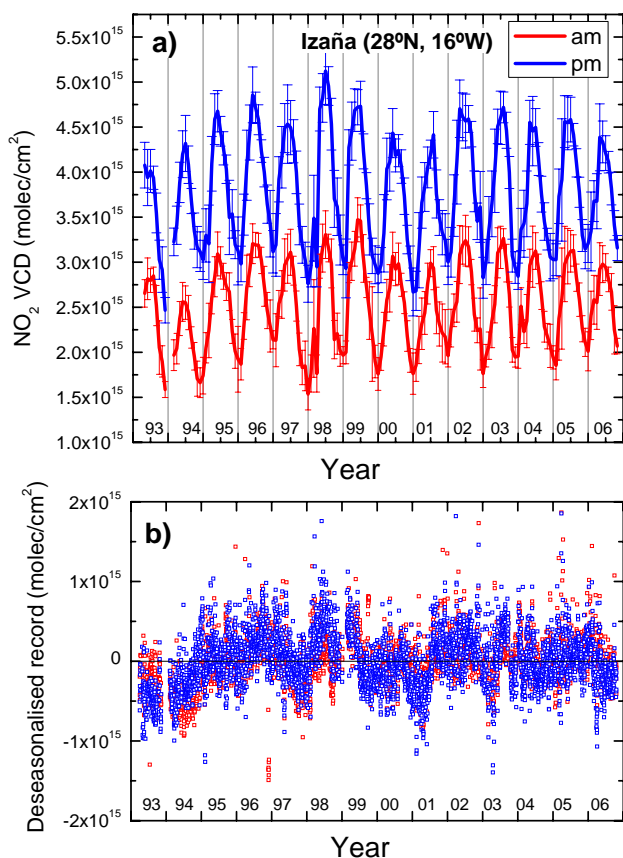
Fig. 9. (a) NO$_2$ monthly mean VCD for a.m. and p.m. observations from 1993—2006. Error bars represent one standard deviation. **(b)** Deseasonalised departure from monthly mean for a.m. and p.m. data.
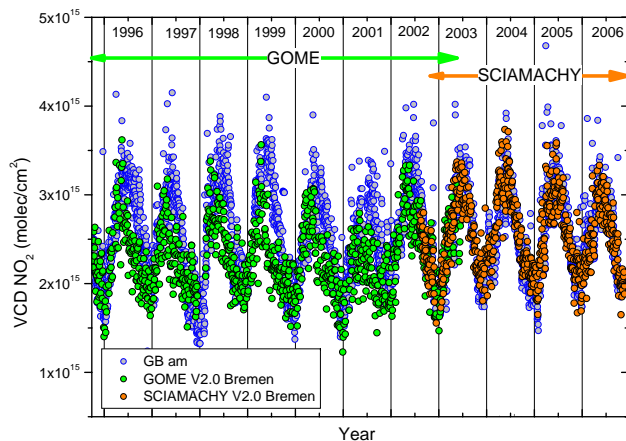

Fig. 10. GOME and SCIAMACHY NO$_2$ VCD from Bremen v2.0 analysis superimposed on ground-based data.

reference (Richter and Burrows, 2002). Therefore, a normalisation over the Pacific region is used assuming a constant NO$_2$ column in that region (Richter et al., 2005a) which
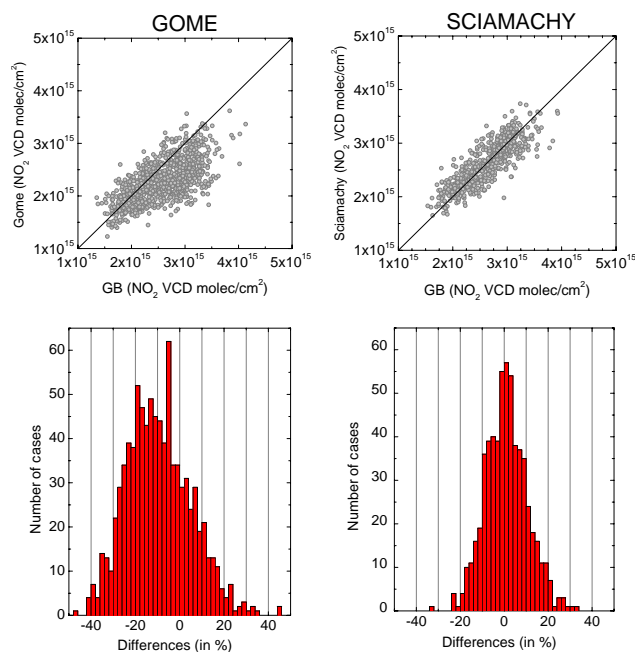

Fig. 11. Satellite – ground-based data cross-correlation (upper panels) and frequency distributions of the differences (lower panels).

strongly limits the information content of GOME measurements at low latitudes. In addition, the Burrows et al. cross-sections used for GOME show differences of up to 10% compared to the cross-sections used for the ground-based measurements which can introduce a corresponding scaling error. The poorer agreement of GOME data compared to SCIA-MACHY (which do not suffer from such an effect) is therefore to be expected.

5.5 Ground-based versus SLIMCAT

Figure 12 shows the comparison of observed and modelled sunrise and sunset column NO$_2$ at Izaña. The chemically free running model (run A) reproduces the general shape of the observed NO$_2$ VCD seasonal cycle but underestimates the magnitude throughout spring and summer. The maximum underestimation is more marked at sunrise (25%) than at sunset (12%). When chemical data assimilation is included (run B) the model-observation comparison improves considerably. The modelled sunrise NO$_2$ VCD now agrees very well in magnitude throughout the annual cycle, although the winter minimum in the observations is overestimated (15%). The sunset agreement is also much better although, as with the sunrise plot, there is an overestimation of the winter minimum seen in the observations (25%). Note that in the assimilation run B the winter minimum is too high.

Clearly, the model run constrained by chemical data assimilation compares better with observations but it is important to bear in mind how that has been achieved and to remember where comparisons are still meaningful. In the case
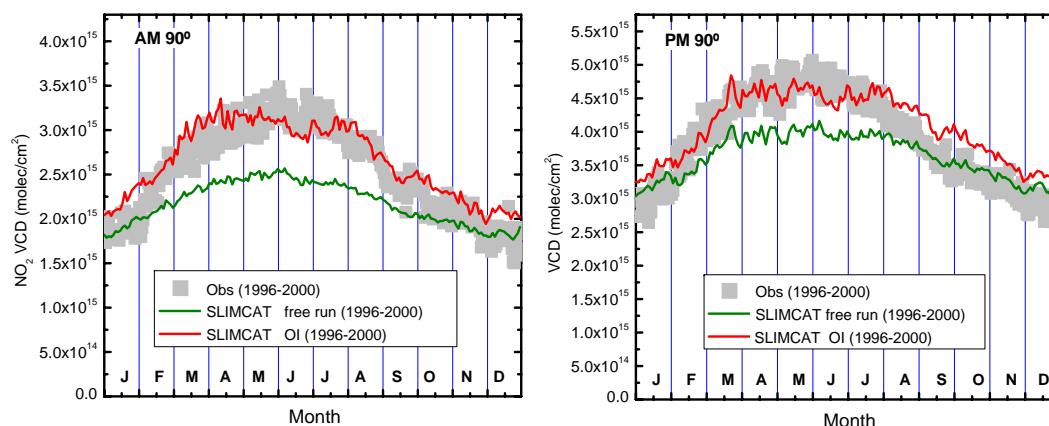
Fig. 12. Mean annual cycle of NO$_2$ VCD at Izaña (1996–2000) for **(a)** a.m. and **(b)** p.m. compared with SLIMCAT 3D CTM runs A (green) and B (red).

of run B, assimilation of HALOE CH$_4$ constrains this modelled field to mimic the observations. Through preserved tracer-tracer correlations the modelled N$_2$O field is transformed and then so is NO$_y$. In effect the CH$_4$ constraint modifies the model NO$_y$ distribution to be consistent. These changes to the long-lived tracers are correcting errors in the modelled transport. The partitioning of chemical species within the NO$_y$ family is then controlled by the model chemistry, as before, although changes to the model O$_3$ through assimilation will affect this slightly. Overall we can say that the assimilation run B is therefore still testing the model NO$_y$ chemistry but, compared to run A, has been corrected for uncertainties in modelled transport.

Figure 12 indicates, therefore, that chemical assimilation improves upon the transport in the model which is determined by the quality of the winds used to force it. There are known problems with the ability of assimilated winds to represent transport in the sub-tropics; analyses tend to allow too much transport from the tropics to mid-latitudes (e.g. Schoeberl et al., 2003).

Clearly, both model runs capture the seasonal cycle in column NO$_2$, although run A underestimates the summer maximum due to transport errors. Run B has improved upon run A, in effect having been corrected for these transport errors. However, run B overestimates the winter minimum by 10% at sunrise and 20% at sunset. In run B the modelled NO$_2$ column generally increases relative to run A because of larger NO$_2$ mixing ratios in the lower stratosphere associated with larger NO$_y$ (and smaller N$_2$O). Without suitable observations (e.g. profiles of NO$_y$ and N$_2$O$_5$) it is not possible to confirm the accuracy of the other model NO$_y$ species and explain the reason for the overestimate in winter column NO$_2$.

6 Summary

Fourteen years of daily NO$_2$ vertical column density (VCD) measurements by zenith sky spectroscopy at the unpolluted NDACC station of Izaña (28° N, 16° W, 2370 m a.s.l.) starting in 1993 have been used to analyse the NO$_2$ climatology in the northern subtropics from diurnal to interannual timescales. The overall uncertainty in the data is estimated to be 12–14% considering measurement errors, cross-section uncertainties and Air Mass Factor approximations.

The NO$_2$ VCD from continuous measurements between 95° a.m. to 95° p.m. displays a diurnal cycle in good agreement with a vertically integrated gas-phase chemical box model, providing observational evidence that the diurnal cycle at low latitudes is dominated by solar radiation via the NOx partitioning. The seasonal cycle is mainly controlled by the available hours of sunlight, but modulated by the temperature in the upper stratosphere. This secondary annual wave contributes 6% to the total column and is phase-shifted by 3 months (maximum in spring) with respect to the solar wave resulting in a shifting of the NO$_2$ VCD maximum toward spring and a flatness of the summer maximum and winter minimum. Mean values are of 2.51×10^{15} and 3.79×10^{15} molec cm^{-2} for a.m. and p.m., respectively. Interannual variability of up to 10% in the annual maxima is observed from the monthly mean record but no trend can be inferred from the available dataset.

Ground-based data have been compared with the GOME (ERS2) and SCIAMACHY (ENVISAT) orbital spectrometers in nadir-viewing mode processed by the University of Bremen (v2.0). SCIAMACHY NO$_2$ VCDs yield an excellent agreement with ground-based data while GOME displays too low values in summer due to a spectral interference pattern induced by the diffuser plate. Mean differences (ground-based minus satellite) are +1.1% for SCIAMACHY and −9.6% for GOME.

Additionally, a comparison between data and modelling has been carried out using long-term output of the SLIM-CAT 3-D CTM. The basic, chemically free running model run A, forced by ECMWF (ERA-40) analyses, captures the observed NO$_2$ annual cycle but significantly underestimates the spring/summer maximum. A second model run B, which assimilated HALOE profiles of CH$_4$ to constrain the model long-lived tracers, showed much better agreement. This improvement in modelled column NO$_2$ is likely due to better modelled NO$_y$ profiles and confirms previously established transport errors in the ECMWF ERA-40 reanalyses. The impact of this on CTM studies of long-term trends in NO$_2$ and O$_3$ needs further investigation.

Edited by: V. F. McNeill

References

Bernhard, G., Evans, R. D., Labow, G. J., and Oltmans, S. J.: Bias in Dobson total ozone measurements at high latitudes due to approximations in calculations of ozone absorption coefficients and air mass, J. Geophys. Res., 110, D10305, doi:10.1029/2004JD005559, 2005.

Bovensmann, H., Burrows, J. P., Buchwitz, M., Frerick, J., Noël, S., Rozanov, V. V., Chance, K. V., and Goede, A. H. P.: SCIA-MACHY – Mission objectives and measurement modes, J. Atmos. Sci., 56(2), 127–150, 1999.

Bogumil, K., Orphal, J., Flaud, J.-M., and Burrows, J.-P.: Vibrational progressions in the visible and near ultraviolet absorption spectrum of ozone, Chem. Phys. Lett., 349, 241–248, 2001.

Bogumil, K., Orphal, J., Homann, T., Voigt, S., Spietz, P., Fleischmann, O. C., Vogel, A., Hartmann, M., Bovensmann, H., Frerick, J., and Burrows, J. P.: Measurements of molecular absorption spectra with the SCIAMACHY pre-flight model: Instrument characterization and reference data for atmospheric remotesensing in the 230–2380 nm region, J. Photoch. Photobio. A, 157, 167–184, 2003.

Brewer, A. W., McElroy C. T., and Kerr, J. B.: Nitrogen dioxide concentration in the atmosphere, Nature, 246, 129–133, 1973.

Burrows, J. P., Dehn, A., Deters, B., Himmelmann, S., Richter, A., Voigt, S., and Orphal, J.: Atmospheric remote-sensing reference data from GOME: Part 1. Temperature-dependent absorption cross-sections of NO$_2$ in the 231–794 nm range, J. Quant. Spectrosc. Ra., 60, 1025–1031, 1998.

Chipperfield, M. P.: Multiannual simulations with a three-dimensional chemical transport model, J. Geophys. Res., 104, 1781–1805, 1999.

Chipperfield, M. P., Khattatov, B. V., and Lary, D. J.: Sequential assimilation of stratospheric chemical observations in a three-dimensional model, J. Geophys. Res. 107, 4585, doi:10.1029/2002JD002110, 2002.

Chipperfield, M. P.: New Version of the TOMCAT/SLIMCAT Off-Line Chemical Transport Model: Intercomparison of Stratospheric Tracer Experiments, Q. J. Roy Meteor. Soc., 132, 1179–1203, doi:10.1256/qj.05.51, 2006.

Denis, L., Roscoe, H. K., Chipperfield, M. P., Van Roozendael, M., and Goutail, F.: A new software suite for NO$_2$ vertical profile retrieval from ground-based zenith-sky spectrometers, J. Quant. Spectrosc. Ra., 92, 3, 321–333, 2005.

Dobber, M. R., Dirksen, R., Voors, R., Mount, G. H., and Levelt, P.: Ground-based zenith sky abundances and in situ gas cross sections for ozone and nitrogen dioxide with the Earth Observing System Aura Ozone Monitoring Instrument, Appl. Optics, 44, 2846–2856, 2005.

ESA (European Space Agency): GOME Global Ozone Measuring Experiment Users Manual, ESA SP-1182, ESA/ESTEC, Noordwijk, 1995.

Fayt, C. and Van Roozendael, M.: WinDOAS 2.1. User Manual, IASB-BIRA, 2001.

Feng, W., Chipperfield, M. P., Dorf, M., Pfeilsticker, K., and Ricaud, P.: Mid-latitude Ozone Changes: Studies with a 3-D CTM Forced by ERA-40 Analyses, Atmos. Chem. Phys., 7, 2357–2369, 2007,
http://www.atmos-chem-phys.net/7/2357/2007/.

Greenblatt, G. D., Orlando, J. J., Burkholder, J. B., and Ravishankara, A. R.: Absorption Measurements of Oxygen Between 330 and 1140 nm, J. Geophys. Res., 95, 18 577–18 581, 1990.

Hendrick, F., Van Roozendael, M., Lambert, J.-C., and de Mazière, M.: Validation of MIPAS NO$_2$ profiles and columns using ground-based zenith-sky UV-visible observations, Geophys. Res. Abstr., 6, 10-2-2004, EGU 2004.

Johnston, P. V., McKenzie, R. L., Keys, J. G., and Matthews, W. A.: Observations of depleted stratospheric NO$_2$ following the Pinatubo volcanic eruption, Geophys. Res. Lett., 19, 211–213, 1992.

Khattatov, B. V., Lamarque, J. F., Lvjak, L. V., Menard, R., Levelt, P., Tie, X. X., Brasseur, G. P., and Gille, J. C.: Assimilation of satellite observations of long-lived chemical species in global chemistry transport models, J. Geophys. Res., 105, 29 135–29 144, 2000.

Koike, M., Kondo, Y., Matthews, W. A., Johnston, P. V., and Yamazaki, K.: Decrease of stratospheric NO$_2$ at 44° N caused by Pinatubo Volcanic aerosols, Geophys. Res. Lett., 20, 1975–1978, 1993.

Lambert, J.-C., Van Roozendael, M., Simon, P. C., De Mazière, M., Pommereau, J.-P., Goutail, F., and Sarkissian, A.: Pole-to-pole validation of GOME level-2 products with ground-based networks, Earth Observation Quarterly, 58, 6–8, 1998.

Lambert, J.-C., Granville, J., Van Roozendael, M., Müller, J.-F., Goutail, F., Pommereau, J.-P., Sarkissian, A., Johnston, P. V., and Russell III, J. M.: Global Behavior of Atmospheric NO$_2$ as Derived from the Integrated Use of Satellite, Ground-based Network and Balloon Observations, Atmospheric Ozone, XIX

Quadrennial Ozone Symposium, Sapporo, Hokkaido, Japan, 3–8 July 2000.

Lambert, J.-C., Blumenstock, T., Boersma, F., Bracher, A., De Maziere, M., Demoulin, P., De Smedt, I., Eskes, H., Gil, M., Goutail, Granville, J., F., Hendrick, F., Ionov, D. V., Johnston, P. V., Kostadinov, I., Kreher, K., Kyrö, E., Martin, R., Meier, A., Navarro-Comas, M., Petritoli, A., Pommereau, J.-P., Richter, A., Roscoe, H. K., Sioris, C., Sussmann, R., Van Roozendael, M., Wagner, T., Wood, S., and Yela, M.: Geophysical validation of SCIAMACHY NO2 vertical columns: overview of early 2004 results, Proc. of the Second Workshop on the Atmospheric Chemistry Validation of ENVISAT (ACVE-2), ESA ESRIN, Frascati, Italy, 3–7 May 2004, ESA SP-562, 2004.

Lambert, J.-C., Granville, J., Hendrick, F., Andersen, S. B., Dorokhov, V., Gerard, P., Gil, M., Goutail, F., Gruzdev, A. N., Held, G., Ionov, D. V., Johnston, P. V., Kostadinov, I., Kreher, K., Kyro, E., Lerot, C., Leveau, J., Navarro-Comas, M., Petritoli, A., Pommereau, J.-P., Richter, A., Roscoe, H. K., Semenov, V. K., Stebel, K., Van Roozendael, M., Vaughan, G., Wagner, T., Wittrock, F., and Yela, M.: Transfer of GOME Data Processor (GDP) version 4.0 to SCIAMACHY Off-line (OL) processor version 3.0: Pole-to-pole delta-validation of NO$_2$ column data with the NDACC/UV-Visible network, Proc. of the Third Workshop on the Atmospheric Chemistry Validation of Envisat (ACVE-3), ESA SP-642, 2007.

Lee, A. M., Roscoe, H. K., Oldham, D. J., Squires, J. A. C., Sarkissian A., and Pommereau, J.-.P.: Improvements to the accuracy of measurements of NO$_2$ by zenith-sky visible spectrometers, J. Quant. Spectrosc. Ra., 52, 5, 649–657, 1994.

Liley, J. B., Johnston, P. V., McKenzie, R. L., Thomas, A. J., and Boyd, I. S.: Stratospheric NO$_2$ variations from a long time series at Lauder, New Zealand, J. Geophys. Res., 105(D9), 11 633–11 640, doi:10.1029/1999JD901157, 2000.

Minschwaner, K., Salawitch, R., and McElroy, M.: Absorption of solar radiation by O$_2$: Implications for O$_3$ and lifetimes of N$_2$O, CFCl$_3$ and CF$_2$Cl$_2$, J. Geophys. Res., 98, 10 543–10 561, 1993.

NDACC: http://www.ndsc.ncep.noaa.gov/, last access: March 2008, 2007.

Noxon, J. F.: Nitrogen Dioxide in the stratosphere and troposphere measured by ground-based absorption spectroscopy, Science, 189, 547–549, 1975.

Orphal, J. A.: Critical Review of the Absorption Cross-Sections of O$_3$ and NO$_2$ in the 240–790 nm Region, Part 2. Nitrogen Dioxide, ESA Technical Note MO-TN-ESA-GO-0302, 2002.

Piters, A. J. M., Bramstedt, K., Lambert, J.-C., and Kirchhoff, B.: Overview of SCIAMACHY validation: 2002–2004, Atmos. Chem. Phys., 6, 127–148, 2006, http://www.atmos-chem-phys.net/6/127/2006/.

Richter, A. and Burrows, J. P.: Retrieval of Tropospheric NO$_2$ from GOME Measurements, Adv. Space Res., 29(11), 1673–1683, 2002.

Richter, A., Wittrock, F., Weber, M., Beirle, S., Kühl, S., Platt, U., Wagner, T., Wilms-Grabe, W., and Burrows, J. P.: GOME observations of stratospheric trace gas distributions during the splitting vortex event in the Antarctic winter 2002 Part I: Measurements, J. Atmos. Sci., 62(3), 778–785, 2005a.

Richter, A., Burrows, J. P., Nüß, H., Granier, C., and Niemeier, U.: Increase in tropospheric nitrogen dioxide over China observed from space, Nature, 437, 129–132, doi:10.1038/nature04092, 2005b.

Richter, A., Kreher, K., Johnston, P. V., Wittrock, F., and Burrows, J. P.: Validation of GOME O$_3$, NO$_2$, BrO, and OClO Measurements in Southern High Latitudes, Procc. of the Fifth European Workshop on Stratospheric Ozone, European Commission, Air Pollution research report 73, 719–722, 2000.

Richter, A., Burrows, J. P., Fietkau, S., Medeke, T., Notholt, J., Oetjen, H., Sierk, B., Warneke, T., Wittrock, F., Dix, B., Friess, U., Wagner, T., Blumenstock, T., Griesfeller, A., Sussmann, R., Rockmann, A., and Schultz, A.: A Scientific NO$_2$ product from Sciamachy: First Results and validation. Proc. of the Second Workshop on the Atmospheric Chemistry Validation of ENVISAT (ACVE-2), ESA ESRIN, Frascati, Italy, 3–7 May 2004, ESA SP-562, 2004.

Rinsland, C. P., Weisenstein, D. K., Ko, M. K. W., Scott, C. J., Chiou, L. S., Mahieu, E., Zander, R., and Demoulin, P.: Post-Mount Pinatubo eruption ground-based infrared stratospheric column measurements of HNO$_3$, NO, and NO$_2$ and their comparison with model calculations, J. Geophys. Res., 108(D15), 4437, doi:10.1029/2002JD002965, 2003.

Roscoe, H. K., Johnston, P. V., Van Roozendael, M., Richter, A., Sarkissian, A., Roscoe, J., Preston, K. E., Lambert, J. C., Hermans, C., Decuyper, W., Dzienus, S., Winterrath, T., Burrows, J., Goutail, F., Pommereau, J. P., D'Almeida, E., Hottier, J., Coureul, C., Didier, R., Pundt, I., Bartlett, L. M., McElroy, C. T., Kerr, J. E., Elokhov, A., Giovanelli, G., Ravegnani, F., Premuda, M., Kostadinov, I., Erle, F., Wagner, T., Pfeilsticker, K., Kenntner, M., Marquard, L. C., Gil, M., Puentedura, O., Yela, M., Arlander, D. W., Kastad Hoiskar, B. A., Tellefsen, C. W., Karlsen Tornqvist, K., Heese, B., Jones, R. L., Aliwell, S. R., and Freshwater, R. A.: Slant column measurements of O3 and NO2 during the NDSC intercomparison of zenith-sky UV-visible spectrometers in june 1996, J. Atmos. Chem., 32, 281–314, 1999.

SAOZ: http://www.aero.jussieu.fr/themes/CA/Reseau_SAOZ.html, 2007.

Sarkissian, A., Fish, D., Van Roozendael, M., Gil, M., Chen, H. B., Wang, P., Pommereau, J. P., and Lenoble, J.: Ozone and NO$_2$ air-mass factors for zenith-sky spectrometers: Intercomparison of calculations with different radiative transfer models, Geophys. Res. Lett., 22, 1113–1116, 1995a.

Sarkissian, A., Roscoe, H. K., and Fish, D.: Ozone measurements by zenith-sky spectrometers: an evaluation of errors in air-mass factors calculated by radiative transfer models, J. Quant. Spectrosc. Ra., 54, 471–480, 1995b.

Schneider, M., Blumenstock, T., Chipperfield, M. P., Hase, F., Kouker, W., Reddmann, T., Ruhnke, R., Cuevas, E., and Fischer, H.: Subtropical trace gas profiles determined by ground-based FTIR spectroscopy at Izaña (28° N, 16° W): Five-year record, error analysis, and comparison with 3-D CTMs, Atmos. Chem., Phys., 5, 153–167, 2005.

Solomon, S., Russell III, J. M., and Gordley, L. L.: Observations of the diurnal variation of Nitrogen dioxide in the stratosphere, J. Geophys. Res., 91(D5), 5455–5464, 1986.

Solomon, S., Schmeltekopft, A. L., and Sanders, R. W.: On the interpretation of zenith sky absorption measurements, J. Geophys. Res., 92(D7), 8311–8319, 1987.

Solomon, S., Sanders, R. W., Jakoubek, R. O., Arpag, K. H., Stephens, S. L., Keys, J. G., and Garcia, R. R.: Visible and near-ultraviolet spectroscopy at McMurdo Station, Antarctica. 10. Re-

ductions of statospheric NO$_2$ due to Pinatubo aerosols, J. Geophys. Res., 99(D2), 3509–3516, 1994.

Struthers, H., Kreher, K., Austin, J., Schonfield, R., Bodecker, G., Johnston, P., Shiona, H., and Thomas, A.: Past and future suimulations of NO$_2$ from a coupled chemistry-climate model in comparison with observations, Atmos. Chem. Phys., 4, 2227–2239, 2004,
http://www.atmos-chem-phys.net/4/2227/2004/.

Sussmann, R., Stremme, W., Burrows, J. P., Richter, A., Seiler, W., and Rettinger, M.: Stratospheric and tropospheric NO$_2$ variability on the diurnal and annual scale: a combined retrieval from ENVISAT/SCIAMACHY and solar FTIR at the Permanent Ground-Truthing Facility Zugspitze/Garmisch, Atmos. Chem. Phys., 5, 2657–2677, 2005,
http://www.atmos-chem-phys.net/5/2657/2005/.

Van Roozendael, M., De Mazière, M., Hermans, C., Simon, P. C., Pommereau, J.-P., Goutail, F., Tie, X.X., Brasseur, G., and Granier, C.: Ground-Based observations of stratospheric NO$_2$ at high and mid-latitudes in Europe after the Mount Pinatubo eruption, J. Geophys Res., 102(D15), 19 171–19 176, 1997.

Vandaele, A. C., Hermans, C., Simon, P .C., Carleer, M., Colins, R., Fally, S., Mérienne, M. F., Jenouvrier, A., and Coquart, B.: Measurements of the NO$_2$ absorption cross-sections from 42000 cm^{-1} to 10000 cm^{-1} (238–1000 nm) at 220 K and 294 K, J. Quant. Spectrosc. Radiat. Transfer, 59, 171–184, 1998.

Vandaele, A. C., Fayt, C., Hendrick, F., Hermans, C., Humbled, F., Van Roozendael, M., Gil, M., Navarro, M., Puentedura, O., Yela, M., Braathen, G., Stebel, K., Tørnkvist, K., Johnston, P., Kreher, K., Goutail, F., Mieville, A., Pommereau, J.-P., Khaikine, S., Richter, A., Oetjen, H., Wittrock, F., Bugarski, S., Friess, U., Pfeilsticker, K., Sinreich, R., Wagner, T., Corlett, G., and Leigh, R.: An intercomparison campaign of ground-based UV-Visible measurements of NO$_2$, BrO, and OClO slant columns. I. NO$_2$, J. Geophys. Res., 110(D8), D08305, doi:10.1029/2004JD005423, 2005.

Wetzel, G., Bracher, A., Funke, B., Goutail, F., Hendrick, F., Lambert, J.-C., Mikuteit, S., Piccolo, C., Pirre, M., Bazureau, A., Belotti, C., Blumenstock, T., De Mazière, M., Fischer, H., Huret, N., Ionov, D., López-Puertas, M., Maucher, G., Oelhaf, H., Pommereau, J.-P., Ruhnke, R., Sinnhuber, M., Stiller, G., Van Roozendael, M., and Zhang, G.: Validation of MIPAS-ENVISAT NO$_2$ operational data, Atmos. Chem. Phys., 7, 3261–3284, 2007, http://www.atmos-chem-phys.net/7/3261/2007/.

WMO (World Meteorological Organization): Scientific Assessment of Ozone Depletion, 2002, Global Ozone Research and Monitoring Project, Report No. 47, 2003.

WMO (World Meteorological Organization): Scientific Assessment of Ozone Depletion: 2006, Global Ozone Research and Monitoring Project, Report No. 50, 2007.

Yela, M., Gil, M., Navarro, M., Rodriguez, S., Cuevas E., and Romero, C.: Meridional transport in the subtropics during winter as seen by NO$_2$ column record, Air Pollution Report 66, EUR 18032EN, edited by: Harris, N. R. P., Kilbane-Dawe, I., and Amanatidis, G. T., 88–91, 1998.

Yela., M., Gil, M., Rodríguez, S., Araujo, J., Ochoa, H., Díaz, S., and Deferrari, G.: Unusual behavior of stratospheric NO$_2$ during splitting vortex event in the Antarctic winter 2002: Comparison with a 10-years NO$_2$ climatology at three Antarctic and sub Antarctic sites, Proc. Quadrennial Ozone Symposium, 1055, 1–8 June 2004, Kos, Greece, 2004.